NEOPLASIA
www.neoplasia.com

Volume 11 Number 9 September 2009 pp. 856–863 856

Molecular Ultrasound Imaging of Early Vascular Response in Prostate Tumors Irradiated with Carbon Ions

Moritz Palmowski[*,†,1], Peter Peschke[‡,1], Jochen Huppert[§], Peter Hauff[¶], Michael Reinhardt[¶], Mathias Maurer[#], Christian P. Karger[**], Michael Scholz[††], Wolfhard Semmler[§], Peter E. Huber[‡] and Fabian M. Kiessling[*]

*Institute of Experimental Molecular Imaging, RWTH-Aachen University, Aachen, Germany; †Department of Diagnostic Radiology, RWTH-Aachen University, Aachen, Germany; ‡Department of Radiation Oncology, German Cancer Research Center and University Hospital Center, Heidelberg, Germany; §Medical Physics in Radiology, German Cancer Research Center, Heidelberg, Germany; ¶Global Drug Discovery, Bayer Schering Pharma AG, Berlin, Germany; #Department of Neurology, Erlangen University, Erlangen, Germany; **Medical Physics in Radiation Oncology, German Cancer Research Center, Heidelberg, Germany; ††Gesellschaft für Schwerionenforschung (GSI), Darmstadt, Germany

Abstract

Individualized treatments with combination of radiotherapy and targeted drugs require knowledge about the behavior of molecular targets after irradiation. Angiogenic marker expression has been studied after conventional radiotherapy, but little is known about marker response to charged particles. For the very first time, we used molecular ultrasound imaging to intraindividually track changes in angiogenic marker expression after carbon ion irradiation in experimental tumors. Expression of intercellular adhesion molecule-1 (ICAM-1) and of $\alpha_v\beta_3$-integrin in subcutaneous AT-1 prostate cancers in rats treated with carbon ions (16 Gy) was studied using molecular ultrasound and immunohistochemistry. For this purpose, cyanoacrylate microbubbles were synthesized and linked to specific ligands. The accumulation of targeted microbubbles in tumors was quantified before and 36 hours after irradiation. In addition, tumor vascularization was analyzed using volumetric Doppler ultrasound. In tumors, the accumulation of targeted microbubbles was significantly higher than in nonspecific ones and could be inhibited competitively. Before irradiation, no difference in binding of $\alpha_v\beta_3$-integrin–specific or ICAM-1–specific microbubbles was observed in treated and untreated animals. After irradiation, however, treated animals showed a significantly higher binding of $\alpha_v\beta_3$-integrin–specific microbubbles and an enhanced binding of ICAM-1–specific microbubbles than untreated controls. In both groups, a decrease in vascularization occurred during tumor growth, but no significant difference was observed between irradiated and nonirradiated tumors. In conclusion, carbon ion irradiation upregulates ICAM-1 and $\alpha_v\beta_3$-integrin expression in tumor neovasculature. Molecular ultrasound can indicate the regulation of these markers and thus may help to identify the optimal drugs and time points in individualized therapy regimens.

Neoplasia (2009) 11, 856–863

Introduction

The recent development of novel antiangiogenic drugs holds great promise for cancer treatment [1]. In previous studies, we and others have shown that radiotherapy can be beneficially combined with inhibitors for vascular endothelial growth factor/platelet-derived growth

Address all correspondence to: Moritz Palmowski, MD, Institute of Experimental Molecular Imaging, RWTH-Aachen University, Pauwelsstraße 30, 52074 Aachen, Germany.
E-mail: mpalmowski@ukaachen.de
[1]These authors contributed equally to this work.
Received 30 March 2009; Revised 10 June 2009; Accepted 12 June 2009

DOI 10.1593/neo.09540

factor signaling [2,3] or inhibitors of $\alpha_v\beta_3$-integrin signaling [4]. The beneficial combination might be caused in part by the up-regulation of receptor molecules for proangiogenic factors including vascular endothelial growth factor or basic fibroblast growth factor after irradiation and the subsequent inhibitory effects of the drugs [5]. Likewise, it is known that irradiation induces expression of $\alpha_v\beta_3$-integrin in human endothelium *in vitro* [4] and in the endothelium of tumor vessels [6]. It is conceivable that the increased level of target receptors after radiation, therefore, might even boost the effects of targeted therapy approaches (e.g., humanized monoclonal antibody therapies directed against $\alpha_v\beta_3$-integrin; EMD 121974 [7]) if administered during the highest level of marker expression; however, the ideal way of using this potentially powerful combination of time optimized drug administration concurrently or after irradiation has yet to be determined, particularly with regard to dose- and time-dependent marker up-regulation. Thus, the ability to noninvasively quantify the modulation of target receptors after irradiation would enable adaptation of the targeted drug regimen to the individual molecular tumor profile of a patient.

Several imaging modalities such as positron emission tomography, single photon emission computed tomography, and optical techniques can be used to assess the expression of angiogenic marker molecules such as $\alpha_v\beta_3$-integrin [8–10]. However, their expense, availability, and ionizing radiation limit patient accessibility. In contrast, ultrasound is the most widely used imaging technique, is inexpensive, is portable, and provides noninvasive real-time imaging. In addition, ultrasound has proven to be highly sensitive for the identification of molecular structures when using targeted contrast agents [11,12]. Ultrasound contrast agents consist of stabilized bubbles with a diameter between 1 and 5 μm. Because of their size, they behave hemodynamically like red blood cells and can be directed selectively to specific vascular beds by conjugating targeting ligands (peptides and antibodies) to their surface [13]. In this regard, molecular imaging using targeted microbubbles has been used *in vivo* to assess inflammation, angiogenesis, and thrombus formation [13]. Recently, it was reported that volumetric molecular ultrasound imaging can be used to depict changes in the molecular profile of tumors during untreated growth or antiangiogenic therapy [14].

Whereas the effects of conventional photon irradiation using low linear energy transfer (LET) beams has been studied in a variety of models, little is known about the effects of high LET radiation using charged particles. These high LET beams combine an excellent physical depth-dose profile with an increased relative biologic effectiveness in the target volume. Molecular and cellular mechanisms underlying this increased relative biologic effectiveness are still under investigation [15,16]. This question is important because several large facilities worldwide will open their clinical program in the coming months or years. One of these facilities will be the heavy ion therapy facility in Heidelberg, Germany, where carbon ion beams will be used for clinical patient treatments (expected >1000 patients per year).

Because very little is known about the impact of carbon ions on the tumor endothelium under *in vivo* conditions, we investigated the potential of three-dimensional molecular ultrasound imaging in assessing changes in the expression of the angiogenic marker $\alpha_v\beta_3$-integrin and of the inflammatory marker intercellular adhesion molecule-1 (ICAM-1) in experimental prostate carcinomas in rats after carbon ion therapy. The results were compared with immunohistologic staining and correlated with the changes in tumor vascularization measured by high-frequency power Doppler ultrasound. From this study, we conclude that molecular ultrasound imaging using targeted microbubbles could be used for noninvasive characterization of tumor angiogenesis and assessment of vascular expression of molecular markers after radiation therapy.

Materials and Methods

Preparation of Target-Specific Microbubbles

Air-filled streptavidin-coated cyanoacrylate microbubbles were custom made as described previously [17]. The target specificity of streptavidin-coated microbubbles was generated immediately before their use by adding either 10 μg of biotinylated antirat–ICAM-1 antibodies (Pharmingen, Heidelberg, Germany) or 5 μg of biotinylated RGD peptides (Peptides International, Louisville, KY; both diluted in 50 μl of phosphate-buffered saline) to 250 μl of microbubble suspension (10^8 microbubbles per milliliter). Reagents were allowed to react for 5 minutes at 20°C, resulting in a 300-μl injection volume containing 2.5×10^7 target-specific microbubbles.

Tumor Model and Therapy Regime

All experiments were approved by the governmental review committee on animal care. The Dunning prostate cancer of rats was chosen as the tumor model [18]. The AT-1 subline used in this study forms anaplastic hormone-independent tumors without glandular differentiation. A total of eight adult male Copenhagen rats (body weight, ~180-200 g) were included in the study. AT-1 tumors were inoculated subcutaneously in both hind legs using fragments of donor tumors. Carbon ion irradiation was performed at the heavy ion accelerator of the "Gesellschaft für Schwerionenforschung" in Darmstadt, Germany. An intensity-controlled raster scanner was used to shape the irradiation fields. A total of seven tumor-bearing animals were treated with a 16-Gy single dose of ^{12}C ions. Treatment was constraint to tumors growing in the distal right thigh, whereas the contralateral tumors served as sham-treated controls. During irradiation, animals were positioned on a specially designed rack and maintained under inhalation anesthesia using oxygen and 2.5 vol% sevoflurane. One animal (the nonirradiated one) was used to verify the specificity of antibody- or RGD peptide–conjugated microbubbles. The remaining seven animals were used to investigate the therapeutic effects of carbon ions, either by imaging ($n = 4$) or by immunohistochemistry ($n = 3$).

Tumor Vascularization Assessed by Three-dimensional High-Frequency Doppler Ultrasound

Ultrasound measurements were performed 36 hours before and 36 hours after carbon ion therapy using the VEVO770 microultrasound system (VisualSonics, Toronto, Canada) equipped with the RMV-704 ultrasound probe (Doppler frequency, 30 MHz). For ultrasound examination, the rats were anesthetized by inhaling a mixture of isoflurane (1.5%) and oxygen (98.5%). The anesthetized animals were placed on an examination table, and the tumors were covered with ultrasound gel. An ultrasound transducer, fixed on a motor-driven unit above the animal, moved perpendicular to the beam axis, thereby acquiring consecutive images in power Doppler mode with a slice thickness of 200 μm. A region of interest (ROI) was drawn within every two-dimensional image. Finally, the two-dimensional ultrasound images were reconstructed to a three-dimensional data set. The vascularization within the tumor (determined as percentage of power Doppler–derived color pixels) was measured. Intraindividual changes measured before and after therapy were expressed as change in percentage (%).

Assessment of Marker Expression Using Molecular Ultrasound Imaging

The same animals (n = 4) were then examined by the three-dimensional quantitative molecular ultrasound technique known as sensitive particle acoustic quantification (SPAQ) [19]. A catheter was placed in the tail vein to enable intravenous injections, and the anesthetized animal was fixed on a gel pad (Figure 1). The tumors, implanted subcutaneously on both hind legs, were positioned downwards, starting with the right side. The pad was placed on a navigable motor-table that could be moved in steps of micrometers over a fixed ultrasound transducer (Sector-Scanner S12, Sonos 5500; Philips Medical Systems, Andover, MA). Unspecific microbubbles were injected intravenously through a tail-vein catheter. Subsequently, saline was injected to clear the catheter from microbubbles. Volumetric imaging was performed 7 minutes after microbubble administration, following a previous study in which timing parameters had been optimized [17]. The initial ultrasound scan of the whole tumor volume was followed by three control scans to ensure that no intact microbubbles remained within the tumor. Imaging took in total less than 2 minutes. Subsequently, the animal was turned around to examine the tumor on the left hind leg, without further administration of microbubbles. After this procedure, RGD-conjugated microbubbles were injected, and the animal was scanned with the identical protocol. Subsequently, the same amount of anti–ICAM-1 antibody–conjugated microbubbles was administered. Thirty-six hours after imaging, tumors implanted on the right hind leg were treated with carbon ions as described above. Thirty-six hours after radiation, animals were examined again with an identical protocol.

For postprocessing, a ROI was drawn around the tumor. Stimulated acoustic emission signals within the ROI were automatically quantified and expressed as particle-based color pixels in a ROI. The color pixels within the three-dimensional ROI were counted and expressed as a percentage of the total number of pixels (color pixel density, CPD [%]).

Specificity of ICAM-1 Antibody– and RGD Peptide–Conjugated Microbubbles

To demonstrate the specificity of the microbubbles, comparative *in vivo* experiments were performed in one animal. The animal first received ICAM-1 antibody–conjugated microbubbles and was scanned by SPAQ. After imaging, it received 200 μg of "nonbiotinylated" ICAM-1 antibodies (Pharmingen) to block the target. Subsequently, ICAM-1 antibody–conjugated microbubbles were administered again, and their accumulation within the tumor was investigated. The same procedure

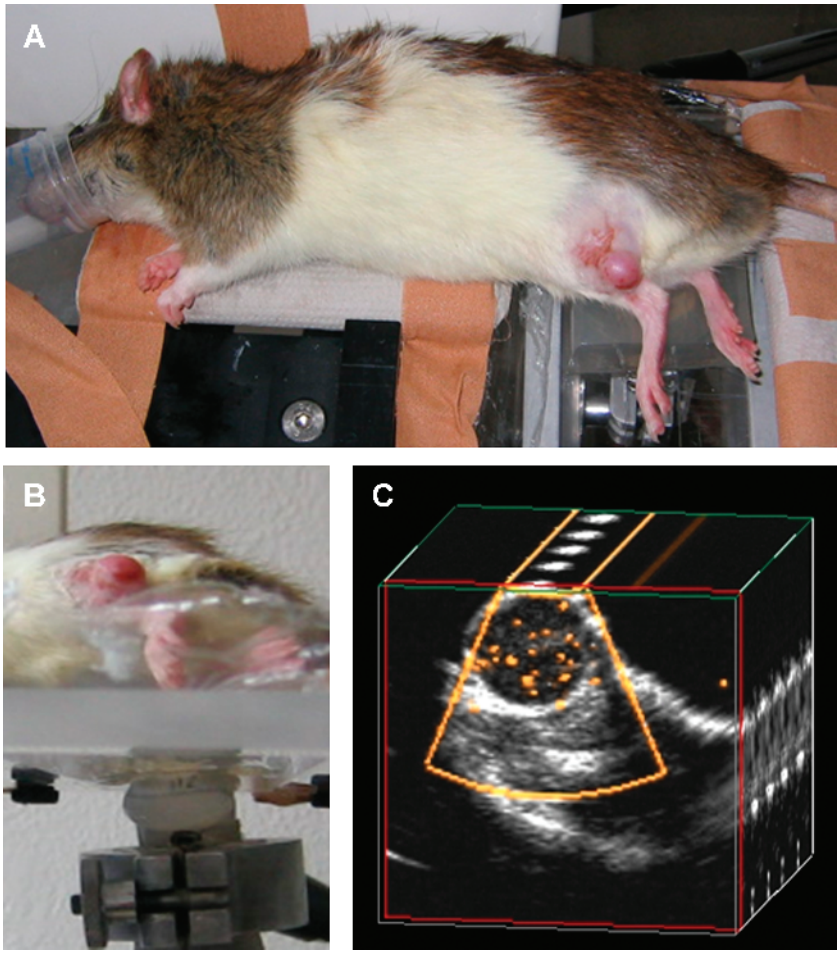

Figure 1. SPAQ-based molecular imaging. (A) A rat with Dunning R3327-AT1 tumors implanted subcutaneously on both hind legs (white arrows) was placed on an ultrasound gel pad. (B) An ultrasound transducer was fixed under the navigable table, which can be moved in micrometer steps. The frame rate of the ultrasound Doppler system (25 Hz) was synchronized with the movement of the table (1.25 mm/sec), resulting in an incremental move of 50 μm between the consecutive ultrasound pulses. (C) During the ultrasound scan, the targeted microbubbles disintegrate and emit detectable signals (yellow dots within the tumor). The two-dimensional ultrasound images are reconstructed to a three-dimensional data set that is quantitatively analyzed by an automatic video densitometry system.

was performed with RGD-conjugated microbubbles and "nonbiotinylated" RGD peptides (R&D Systems, Minneapolis, MN).

As additional negative controls, the animal received microbubbles conjugated to biotinylated mouse–antihuman immunoglobulin G (IgG) control antibodies (antibodies-online GmbH, Aachen, Germany) and to amino-terminal–biotinylated RAD peptides (Biotin-GRADSP; Biomol GmbH, Hamburg, Germany). Their accumulation within the tumor neovasculature was investigated and compared with the specific microbubbles as well as with unconjugated microbubbles.

Immunohistochemistry

Three separate animals were killed for immunohistochemical analysis. Irradiated and control tumors were removed surgically. Tumors were frozen in liquid nitrogen vapor, cut in sections, and fixed by methanol/acetone. Immunostaining was performed for CD31 (endothelial cells; mouse-antirat CD31 IgG; Chemicon International, Temecula, CA), CD61 ($\alpha_v\beta_3$-integrin; mouse-antirat CD61 IgG; Fitzgerald Industries International, Concord, MA), and CD-54 (ICAM-1; mouse-antirat CD54 IgG; BD Biosciences, San Jose, CA). A goat-antimouse IgG antibody conjugated to Alexa Fluor 555 (Gentaur Molecular Products, Brussels, Belgium) served as secondary antibody. Cell nuclei were counterstained by 4′,-6-diamidino-2-phenylindole (Invitrogen, Karlsruhe, Germany). Tissue fluorescence sections were obtained. For the quantitative analysis of fluorescence signals, area fractions with positive fluorescence were calculated. Ten representative area fractions were analyzed from each tumor in the control and therapy groups.

Statistical Evaluation

Data are presented as mean ± SD. Differences in microbubble concentrations and vascularization between treated and untreated tumors were compared using the Mann-Whitney test (2-tailed). $P < .05$ was considered significant. Statistical analysis was performed using GraphPadPrism 5.0 (GraphPad Software, San Diego, CA).

Results

Specificity of Targeted Mircobubbles

The concentrations of unspecific microbubbles as well as ICAM-1–specific and $\alpha_v\beta_3$-integrin–specific microbubbles in tumors could be quantified *in vivo* simultaneously (Figure 1) by destroying stationary microbubbles through a volumetric high-powered Doppler ultrasound scan. The number of voxels containing power Doppler signals was normalized to the total number of voxels of the tumor volume to reveal CPD values as a percentage (%).

In line with previous findings [14,17], specific microbubbles accumulated significantly more intensely than unconjugated ones in all tumors ($P = .0006$ for ICAM-1–specific and $P = .01$ for RGD-specific microbubbles; Figure 2). In detail, the highest mean CPD in tumors was found for ICAM-1–specific microbubbles (8.54 ± 3.98%; $n = 8$ tumors) followed by $\alpha_v\beta_3$-integrin–specific microbubbles (5.11 ± 1.83%; $n = 8$ tumors). Nonconjugated microbubbles accumulated significantly less intensely (2.96 ± 1.85%; $n = 8$ tumors).

Non–sense peptide–conjugated microbubbles and IgG control antibody–conjugated microbubbles accumulated even less intensely than unconjugated microbubbles with a free streptavidin coating. However, the difference in retention of uncoated, RAD non–sense peptide–conjugated microbubbles (reduced by a factor of 0.8 compared with unconjugated microbubbles), and IgG control antibody–conjugated microbubbles (reduced by a factor of 0.75 compared with unconjugated microbubbles) was too small to reach statistical significance.

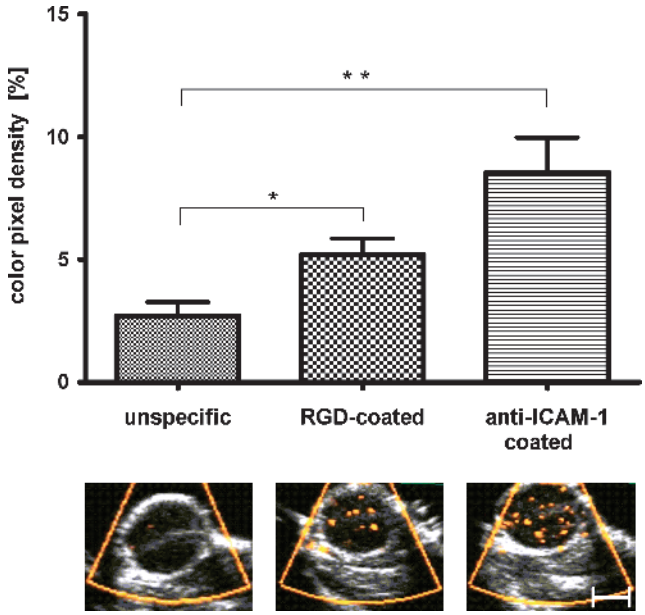

Figure 2. Volumetric SPAQ measurements of entire tumors prove the specificity of targeted microbubbles: After injection of unspecific microbubbles, no relevant accumulation was observed within tumor vessels. After administration of RGD-coated microbubbles targeted against $\alpha_v\beta_3$-integrin, more Doppler signals (yellow dots) were visible, representing the bursting of stationary microbubbles at their target. Quantitative analysis indicated significant accumulation compared with unspecific microbubbles. Accumulation of anti–ICAM-1 antibody–coated microbubbles was even more pronounced (*$P < .05$; **$P < .01$; $n = 8$ tumors).

After administration of free ligands in excess (ICAM-1 antibodies or RGD peptides), binding of specific microbubbles was reduced by a factor of 0.71 for ICAM-1–specific microbubbles and by a factor of 0.61 for $\alpha_v\beta_3$-integrin–specific microbubbles. Hence, competitive blocking of the target could be demonstrated successfully *in vivo*.

To ensure that the signals counted did indeed originate from stationary targeted microbubbles rather than from blood flow or unbound microbubbles within the blood pool, each scan was followed by three control scans. Independent of the ligand that was bound to the microbubbles, a significantly ($P = .0002$) lower CPD was found in the control scans (10.46 ± 4.42% during the first scan *vs* 2.05 ± 0.75%, 1.97 ± 0.74%, and 1.88 ± 0.75% during the consecutive control scans for ICAM-1–conjugated microbubbles). In this context, the reproducibly low concentration of microbubbles in the control scans indicates that all site-targeted microbubbles were destroyed during the first diagnostic scan using high-power sonication.

Tumor Monitoring after Carbon Ion Irradiation by Functional and Molecular Ultrasound

To investigate whether changes in the expression of ICAM-1 or $\alpha_v\beta_3$-integrin on tumor vessels can be assessed by molecular ultrasound, tumors ($n = 4$) on the right hind leg of the animals were investigated 36 hours before and 36 hours after irradiation with carbon ions. Tumors ($n = 4$) implanted on the left hind leg served as untreated controls.

Tumor size. Before therapy, the mean size of tumors in the control and therapy group did not differ significantly (212 ± 68 mm^3 *vs* 272 ± 53 mm^3, respectively). After 72 hours, the mean tumor volume in the control group had increased by 120 ± 36%. In the therapy group, retarded tumor growth with an increase of only 74 ± 38% was found.

Tumor vascularization. Vascularization of the tumors, as determined by volumetric high-frequency power Doppler ultrasound and normalized to the initial value, indicated a comparable decrease in both groups during tumor growth: In detail, the relative blood volume decreased from 100% to 55 ± 6% in the control group and from 100% to 52 ± 15% in the therapy group.

Retention of $\alpha_v\beta_3$-integrin–specific microbubbles. Before treatment, no significant difference was found between tumors in the control and treatment groups with regard to retention of $\alpha_v\beta_3$-integrin–specific microbubbles (control group: 6.78 ± 2.81% CPD; treatment group: 7.37 ± 1.26% CPD).

After 3 days, binding of $\alpha_v\beta_3$-integrin–specific microbubbles had decreased in untreated controls to 57% of the original value (day 3: 3.91 ± 1.13% CPD). This decrease is in line with the general decrease in vascularization during this time interval (decrease from 100% to 55 ± 6%; see previous paragraphs).

In irradiated tumors, however, binding of $\alpha_v\beta_3$-integrin–specific microbubbles decreased to only 88% of the original value (day 3: 6.54 ± 1.23% CPD) despite a decrease in vascularization comparable to that found in control tumors. The difference in the accumulation of $\alpha_v\beta_3$-integrin–specific microbubbles between treated and untreated tumors was significant, with higher values in the treatment group ($P < .05$).

Assuming that the general decrease in microbubble retention is somehow related to the general decrease in vascularization, normalization of microbubble accumulation to the relative blood volume was performed. Although over time, normalized data on the accumulation of $\alpha_v\beta_3$-integrin–specific microbubbles do not significantly change in untreated control tumors, significantly increased values are found in irradiated tumors, indicating up-regulation of this marker on the vasculature ($P < .05$; Figures 3 and 4).

Retention of ICAM-1–specific microbubbles. Before treatment, no significant difference was found in the mean accumulated number of stationary ICAM-1–specific microbubbles between tumors of the control and treatment groups (control group: 19.49 ± 3.41% CPD; treatment group: 15.38 ± 2.54% CPD).

After 3 days, binding of ICAM-1–specific microbubbles in the untreated controls had significantly decreased to 38% of the original value (day 3: 7.58 ± 3.79% CPD), most probably because of the decrease in vascularization during this time interval (decrease from 100% to 55 ± 6%; see previous paragraphs). In treated tumors, however, binding of ICAM-1–specific microbubbles decreased to only 61% (day 3: 9.5 ± 4.48% CPD) despite the comparable decrease in vascularization. Differences in the binding of ICAM-1–specific microbubbles in untreated and irradiated tumors were not significant. However, higher values were found in treated tumors than in control ones, whereas at the first examination time point, the opposite had been true.

Normalization of the concentration of ICAM-1–specific microbubbles to the vascularization points to a down-regulation of this marker at the vasculature of control tumors between the first and the second examination time points (Figures 3 and 4).

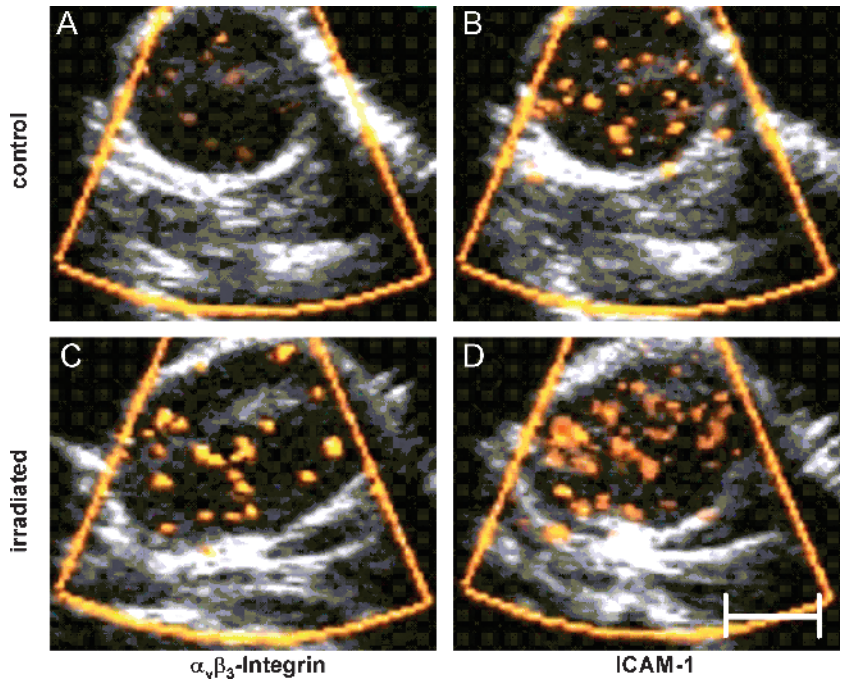

Figure 3. Representative ultrasound images of irradiated and nonirradiated Dunning prostate tumors after injection of targeted microbubbles using a three-dimensional destructive ultrasound technique (SPAQ [19]). Site-targeted microbubbles are color-coded as yellow Doppler signals. (A and C) Retention of $\alpha_v\beta_3$-integrin–specific microbubbles is significantly lower in nonirradiated tumors (A) compared with irradiated ones (C; *$P < .05$). (B and D) Accumulation of ICAM-1–specific microbubbles is lower in nonirradiated tumors (B) compared with irradiated ones (D).

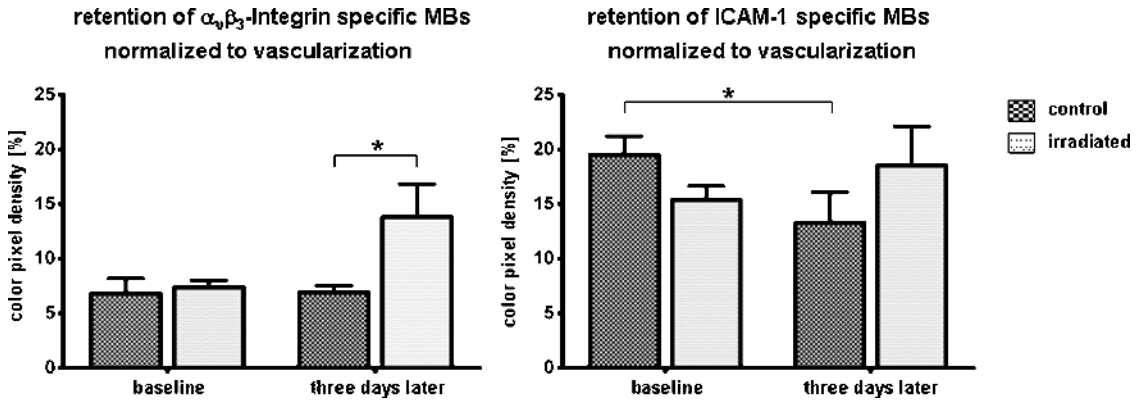

Figure 4. Normalized data showed that retention of $\alpha_v\beta_3$-integrin–specific microbubbles was significantly increased in irradiated tumors, indicating an up-regulation of this marker on tumor vessels. The normalized concentration of ICAM-1–specific microbubbles also increased after irradiation, whereas decreasing values were found in untreated controls.

Carbon Ion Effects in Tumor Neovasculature in Immunohistochemical Analysis

Quantitative analysis of immunofluorescence-positive area fractions revealed that there are no significant differences in the expression of CD31-positive vessels in untreated (2.47 ± 1.59% area fraction) and irradiated (2.27 ± 1.15% area fraction) tumors. However, significantly higher levels of CD61 ($\alpha_v\beta_3$-integrin) and CD54 (ICAM-1) were observed in irradiated tumors. In detail, CD54-positive area fractions were 0.17 ± 0.13% in irradiated tumors and 0.02 ± 0.01% in controls ($P < .01$). Area fractions of CD61-positive staining were 0.07 ± 0.05%

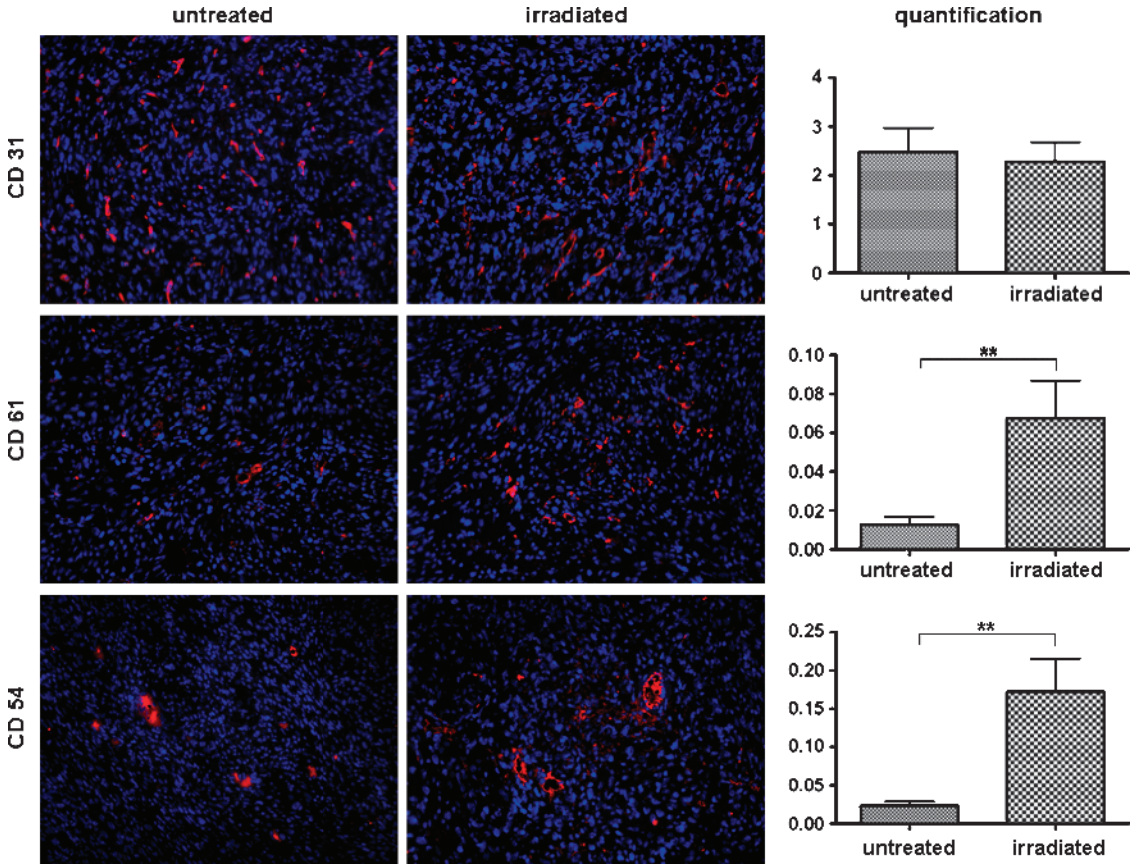

Figure 5. Immunofluorescence images of untreated and irradiated tumors showing cell nuclei stained with Hoechst (blue) and endothelial cells stained with CD31 (red, upper column), $\alpha_v\beta_3$-integrin stained with CD61 (red, middle column), or ICAM-1 stained with CD54 (red, lower column). Quantification of the positive area fractions showed equal expression of CD31 in both groups, whereas CD61 and CD54 were both significantly overexpressed in irradiated tumors. However, it must be mentioned that CD61 and CD54 are expressed not only by endothelial cells but also by a certain number of tumor cells (**$P < .01$).

in irradiated tumors and 0.01 ± 0.01% in controls ($P < .01$). However, one must consider that CD61 and CD54 are expressed not only by endothelial cells but also, to some extent, by tumor cells as well. Therefore, results from quantitative immunohistochemistry reflect the overall up-regulation of CD61 and CD54 in treated tumors after irradiation (Figure 5).

Discussion

Conventional radiotherapy is known to induce an up-regulation of angiogenic marker molecules, which might allow adaptation of complementary targeted treatment approaches [20]. This is the first investigation of carbon ion radiation effects in experimental tumors *in vivo* by noninvasive functional and molecular ultrasound imaging with focus on the vascular changes.

On the basis of immunohistochemical analysis, we found that expression of the angiogenic marker $\alpha_v\beta_3$-integrin and expression of the inflammatory maker ICAM-1 can both be induced by heavy ion irradiation. We observed a general up-regulation of both markers on angiogenic vessels and tumor cells. Moreover, changes in the expression of both markers on endothelial cells could be detected and quantified by molecular ultrasound. However, to correctly interpret the marker regulation, combined assessment of functional and molecular data was required:

Functional ultrasound demonstrated a general decrease in vascularization during 3 days of tumor growth, which affected both treated and untreated tumors. We explain this finding as increased interstitial fluid pressure at the center of the tumor and a loss in vessel functionality, which are both known to occur during tumor growth [21,22]. Likewise, retention of specific microbubbles decreased to an equal degree in control tumors. In irradiated tumors, the retention of specific microbubbles also decreased but to a lower degree than in untreated controls. Tumors treated with carbon ions showed a significantly higher retention of $\alpha_v\beta_3$-integrin–specific microbubbles and a tendency to higher accumulation of ICAM-1–specific microbubbles than in nonirradiated tumors. To better examine the influence of changes in functional vascularization on the accumulation of targeted microbubbles, we normalized the concentrations of stationary microbubbles to the relative blood volume. The resulting data suggested that both markers are strongly upregulated on the vasculature after irradiation, whereas unchanged or even lower expression occurs in untreated tumors.

Combined assessment of the functional and molecular information, as performed in our study, is required to draw conclusions about whether the changing retention of microbubbles is related to a general alteration in vascularization or to a real up- (or down-) regulation of the markers by the endothelial cells. In most previous approaches, information on vessel densities was derived from histologic measurements of CD31-stained area fractions or was not available at all. For example, histologic assessment of the vessel density in combination with imaging of the molecular marker expression in tumor xenografts during matrix metalloproteinase 2/9 inhibitor treatment has recently been reported in an ultrasound study [14]. In contrast to this study, which required invasive data to supplement the noninvasive imaging, Ellegala et al. [23] reported on combined functional and molecular ultrasound imaging during investigations on U87MG tumors in rats. They observed an up-regulation of $\alpha_v\beta_3$-integrin during tumor growth, which correlated to an increase in blood volume. Therefore, the increasing marker densities seemed to reflect the general increase in vessel surface. In contrast to these results, in the present study, we observed, after carbon ion therapy, an up-regulation of the markers on the endothelium over time accompanied with strongly decreasing vascularization.

Increased expression of $\alpha_v\beta_3$-integrin after irradiation has been reported in other studies regarding the effects of x-ray irradiation on endothelial cells [20]. However, little is known about the response of the endothelium to carbon ions. Takahashi et al. [15] investigated the effects of carbon irradiation on human umbilical vein endothelial cells. Interestingly, they reported a down-regulation of $\alpha_v\beta_3$-integrin in contrast with the reported effects of conventional radiotherapy. This observation contrasts with the known effect of conventional radiotherapy [20]. However, the study was performed *in vitro*, and endothelial cells may behave different in tumors or in a physiological matrix. In our *in vivo* setting, we could clearly demonstrate an up-regulation of $\alpha_v\beta_3$-integrin on endothelial cells by immunohistochemistry and targeted ultrasound within a given time window of 36 hours after irradiation. The up-regulation on the tumor cells themselves was assessable solely by immunohistochemistry because ultrasound contrast agents are too large to leave the vascular bed [11–13]. Consequently, targeted ultrasound imaging enables the isolated detection of markers expressed on endothelial cells.

The second marker molecule investigated in our study was the adhesion molecule ICAM-1. ICAM-1 plays a key role in cellular traffic through the capillary wall, particularly during the inflammatory response when leukocytes migrate from blood into tissues [24]. The down-regulation of ICAM-1 in untreated control tumors indicates a decrease in inflammation during a more advanced stage of our experimental prostate carcinomas. In contrast to the down-regulation during growth, we found an up-regulation after irradiation. Inflammation is one of the major consequences of γ-radiation injury, and an up-regulation of ICAM-1 after conventional irradiation has already been reported in the literature [24]. However, for the first time, our results indicate that the expression of the inflammation marker ICAM-1 is also inducible by carbon ions. Therefore, imaging of ICAM-1 expression might be valuable in assessing therapy response or even for giving an early indication of adverse effects (such as radionecrosis). The difference between conventional carbon ions is that conventional radiation therapy uses photons, which are characterized by a low LET into the irradiated tissue [5]. Although the net effect on cells *in vitro* and *in vivo* in general is antiproliferative and proapoptotic, conventional ionizing irradiation may trigger escape mechanisms with upregulated proangiogenic surviving factors through integrins and receptor tyrosine kinases. The combined approach of ionizing radiation with pharmacological antagonists of $\alpha_v\beta_3$-integrin efficiently suppresses angiogenesis in several preclinical models [4,25,26]. One drug, the cyclic Arg-Gly-Asp peptide Cilengitide (EMD 121974) is presently undergoing clinical evaluation alone and in combination with photon [7], supporting the translational relevance of our studies.

In conclusion, carbon ion therapy induces an up-regulation of ICAM-1 and $\alpha_v\beta_3$-integrin after irradiation, which can be assessed noninvasively by three-dimensional molecular ultrasound. However, changes in the vascular functionality that occur during tumor growth require a combination of molecular imaging and assessment of the relative blood volume. In combination, the two methods can be used to elucidate the dose- and time-dependent expression of multiple marker molecules after heavy ion irradiation. It permits adaptation of the therapy regimen to the molecular profile of tumors and their environment and opens new perspectives for individualized timing of combined anticancer therapies and treatment of irradiation-induced adverse effects.

References

[1] Ferrara N and Kerbel RS (2005). Angiogenesis as a therapeutic target. *Nature* **438**, 967–974.

[2] Timke C, Zieher H, Roth A, Hauser K, Lipson KE, Weber KJ, Debus J, Abdollahi A, and Huber PE (2008). Combination of vascular endothelial growth factor receptor/platelet-derived growth factor receptor inhibition markedly improves radiation tumor therapy. *Clin Cancer Res* **14**, 2210–2219.

[3] Huber PE, Bischof M, Jenne J, Heiland S, Peschke P, Saffrich R, Gröne HJ, Debus J, Lipson KE, and Abdollahi A (2005). Trimodal cancer treatment: beneficial effects of combined antiangiogenesis, radiation, and chemotherapy. *Cancer Res* **65**, 3643–3655.

[4] Abdollahi A, Griggs DW, Zieher H, Roth A, Lipson KE, Saffrich R, Gröne HJ, Hallahan DE, Reisfeld RA, Debus J, et al. (2005). Inhibition of $\alpha(v)\beta_3$ integrin survival signaling enhances antiangiogenic and antitumor effects of radiotherapy. *Clin Cancer Res* **11**, 6270–6279.

[5] Abdollahi A, Lipson KE, Han X, Krempien R, Trinh T, Weber KJ, Hahnfeldt P, Hlatky L, Debus J, Howlett AR, et al. (2003). SU5416 and SU6668 decrease angiogenic effects of radiation-induced factor productions by tumor cells and amplify the direct anti-endothelial action of radiation *in vitro*. *Cancer Res* **63**, 3755–3763.

[6] Onoda JM, Piechocki MP, and Honn KV (1992). Radiation-induced increase in expression of the $\alpha_{IIb}\beta_3$ integrin in melanoma cells: effects on metastatic potential. *Radiat Res* **130**, 281–288.

[7] Lode HN, Moehler T, Xiang R, Jonczyk A, Gillies SD, Cheresh DA, and Reisfeld RA (1999). Synergy between an antiangiogenic integrin α_v antagonist and an antibody-cytokine fusion protein eradicates spontaneous tumor metastases. *Proc Natl Acad Sci USA* **96**, 1591–1596.

[8] Beer AJ and Schwaiger M (2008). Imaging of integrin $\alpha_v\beta_3$ expression. *Cancer Metastasis Rev* **27**, 631–644.

[9] Cai W, Rao J, Gambhir SS, and Chen X (2006). How molecular imaging is speeding up antiangiogenic drug development. *Mol Cancer Ther* **5**, 2624–2633.

[10] von Wallbrunn A, Höltke C, Zühlsdorf M, Heindel W, Schäfers M, and Bremer C (2007). *In vivo* imaging of integrin $\alpha_v\beta_3$ expression using fluorescence-mediated tomography. *Eur J Nucl Med Mol Imaging* **34**, 745–754.

[11] Lindner JR (2004). Microbubbles in medical imaging: current applications and future directions. *Nat Rev Drug Discov* **3**, 527–532.

[12] Klibanov AL (2006). Microbubble contrast agents: targeted ultrasound imaging and ultrasound-assisted drug-delivery applications. *Invest Radiol* **41**, 354–362.

[13] Kiessling F, Huppert J, and Palmowski M (2009). Functional and molecular ultrasound imaging: concepts and contrast agents. *Curr Med Chem* **16**, 627–642.

[14] Palmowski M, Huppert J, Ladewig G, Hauff P, Reinhardt M, Mueller MM, Woenne EC, Jenne JW, Maurer M, Kauffmann GW, et al. (2008). Molecular profiling of angiogenesis with targeted ultrasound imaging: early assessment of antiangiogenic therapy effects. *Mol Cancer Ther* **7**, 101–109.

[15] Takahashi Y, Teshima T, Kawaguchi N, Hamada Y, Mori S, Madachi A, Ikeda S, Mizuno H, Ogata T, Nojima K, et al. (2003). Heavy ion irradiation inhibits *in vitro* angiogenesis even at sublethal dose. *Cancer Res* **63**, 4253–4257.

[16] Ogata T, Teshima T, Kagawa K, Hishikawa Y, Takahashi Y, Kawaguchi A, Suzumoto Y, Nojima K, Furusawa Y, and Matsuura N (2005). Particle irradiation suppresses metastatic potential of cancer cells. *Cancer Res* **65**, 113–120.

[17] Palmowski M, Morgenstern B, Hauff P, Reinhardt M, Huppert J, Maurer M, Woenne EC, Doerk S, Ladewig G, Jenne JW, et al. (2008). Pharmacodynamics of streptavidin-coated cyanoacrylate microbubbles designed for molecular ultrasound imaging. *Invest Radiol* **43**, 162–169.

[18] Dunning WF (1963). Prostate cancer in the rat. Biology of the prostate and related tissues. *Natl Cancer Inst Monogr* **12**, 351–369.

[19] Reinhardt M, Hauff P, Briel A, Uhlendorf V, Linker RA, Mäurer M, and Schirner M (2005). Sensitive particle acoustic quantification (SPAQ): a new ultrasound-based approach for the quantification of ultrasound contrast media in high concentrations. *Invest Radiol* **40**, 2–7.

[20] Cao C, Shinohara ET, Subhawong TK, Geng L, Woon Kim K, Albert JM, Hallahan DE, and Lu B (2006). Integrin $\alpha_v\beta_3$ antagonist Cilengitide enhances efficacy of radiotherapy in endothelial cell and non–small-cell lung cancer models. *Int J Radiat Oncol Biol Phys* **65**, 1536–1543.

[21] Heldin CH, Rubin K, Pietras K, and Ostman A (2004). High interstitial fluid pressure—an obstacle in cancer therapy. *Nat Rev Cancer* **4**, 806–813.

[22] Palmowski M, Huppert J, Hauff P, Reinhardt M, Schreiner K, Socher MA, Hallscheidt P, Kauffmann GW, Semmler W, and Kiessling F (2008). Vessel fractions in tumor xenografts depicted by flow- or contrast-sensitive 3D high-frequency Doppler ultrasound respond differently to antiangiogenic treatment. *Cancer Res* **68**, 7042–7049.

[23] Ellegala DB, Leong-Poi H, Carpenter JE, Klibanov AL, Kaul S, Shaffrey ME, Sklenar J, and Lindner JR (2003). Imaging tumor angiogenesis with contrast ultrasound and microbubbles targeted to $\alpha(v)\beta_3$. *Circulation* **108**, 336–341.

[24] Gaugler MH, Squiban C, van der Meeren A, Bertho JM, Vandame M, and Mouthon MA (1997). Late and persistent up-regulation of intercellular adhesion molecule-1 (ICAM-1) expression by ionizing radiation in human endothelial cells *in vitro*. *Int J Radiat Biol* **72**, 201–209.

[25] Allman R, Cowburn P, and Mason M (2000). *In vitro* and *in vivo* effects of a cyclic peptide with affinity for the $\alpha(v)\beta_3$ integrin in human melanoma cells. *Eur J Cancer* **36**, 410–422.

[26] Burke PA, DeNardo SJ, Miers LA, Lamborn KR, Matzku S, and DeNardo GL (2002). Cilengitide targeting of $\alpha(v)\beta(3)$ integrin receptor synergizes with radioimmunotherapy to increase efficacy and apoptosis in breast cancer xenografts. *Cancer Res* **62**, 4263–4272.